Templated Self-Assembly Over Patterned Electrodes by an Applied Electric Field: Geometric Constraints and Diversity of Materials

Adam Winkleman, Logan S. McCarty, Ting Zhu, *Member, ASME*, Douglas B. Weibel, Zhigang Suo, *Fellow, ASME*, and George M. Whitesides

***Abstract*—This paper expands the scope and usefulness of a process to assemble dry micrometer-sized particles into arrays over a templated electrode by a high-voltage dc bias. Using the predictions from a theoretical model for the process of assembly, the experimental scope and limitations of this technique were explored and related to the predictions of the model. The range of bead size that can be assembled (20–750 μm) and the effects of changing the ratio of the size of the features in the templated electrode to the size of the particles being assembled were experimentally determined and compared to the theory. It was also demonstrated that: 1) the assembled spheres can be made of materials that are either dielectrics (glass and polystyrene), semiconductors (silicon), or conductors (copper); 2) the material for the electrode can either be gold, silver, copper, or amorphous silicon; and 3) the dielectric substrate only needs to be able to support the applied voltage without breaking down. The experimental results, in general, were predicted and supported by the model. [2008-0011]**

***Index Terms*—Microassembly.**

I. Introduction

THIS PAPER expands the scope and usefulness of a previously reported process [1] in which dry micrometer-sized particles self-assemble over the windows in a patterned electrode under the influence of an applied electric field. A "window" is a region of an electrode that has been removed by using either soft lithography and etching, or photolithography and liftoff; these processes expose the underlying dielectric substrate (normally polystyrene in this paper). Using the predictions from our theoretical model for the process of assembly (a parallel-plate capacitor with voids in the upper electrode) [2] as our impetus, we rationalized and explored the experimental scope and limitations of this technique and related these observations to predictions from our theoretical model. We examined the parameters characterizing the process to determine the breadth of its applications and its limitations. We also examined the influence of the geometry of the windows on the regularity and yield of the assemblies and determined experimentally a range of geometries that produced highly ordered assemblies. We extended the theory to compute the net force on a particle at various distances from the center of a window and on multiple particles assembling over a single window. We investigated the materials that could be used in this system, and we found that the particles, the electrode, and the dielectric substrate could each be chosen from a wide variety of materials, as predicted by our model.

Generating Regular Structures in Patterns: As components for devices become smaller, new processes for assembling these components become necessary [3], [4]. Current technology for assembling components uses pick-and-place robotics—a serial process that, for small (< 100 μm) components, is slow, costly, and difficult to implement [5]. Self-assembly, which uses global energy minimization and a wide variety of forces, can, in principle, organize components into desired structures using a rapid parallel process [6], [7].

Self-Assembly of MEMS Devices: In addition to designing smaller components for MEMS devices, the incorporation of materials and substrates that are incompatible with traditional methods of fabrication (e.g., flexible plastic substrates) and the desire to design 3-D structures will require other means of integrating system components; in these areas, self-assembly has great potential [4], [8]. Most of the self-assembling systems were accomplished in solution in which the driving force for assembly was capillarity or shape recognition [8]–[14]]. Solder can act as both an adhesive and a method for making electrical connections between components and substrates in the assembly of functional electronic devices including LED arrays [13], logic inverters, [8] and 3-D circuits [10], [14]. Magnetic forces [10], [12] and surface tension [15], [16] have been employed to assemble individual pieces from planar structures into 3-D functional components.

Electrostatic Self-Assembly (ESA): Electrostatic forces have received considerable attention for their potential in self-assembly, although they have not yet been exploited to self-assemble MEMS devices. These forces act over a long range, interact with all materials, and respond readily to applied potentials from external electrodes. The following are the two types of procedures that commonly use ESA: 1) assembling

Manuscript received January 15, 2008. First published June 6, 2008; last published August 1, 2008 (projected). This work was supported by the Army Research Office (W911NF-04-1-0170) and used the shared resource facilities supported by the National Science Foundation under NSEC (PHY-0117795) and MRSEC (DMR-0213805) awards. The work of D. B. Weibel was supported by the National Institutes of Health (GM067445) through a postdoctoral fellowship. Subject Editor L. Spangler.

A. Winkleman, L. S. McCarty, D. B. Weibel, and G. M. Whitesides are with the Department of Chemistry and Chemical Biology, Harvard University, Cambridge, MA 02138 USA (e-mail: gwhitesides@gmwgroup.harvard.edu).

T. Zhu and Z. Suo are with the Division of Engineering and Applied Sciences, Harvard University, Cambridge, MA 02138 USA.

Color versions of one or more of the figures in this paper are available online at http://ieeexplore.ieee.org.

Digital Object Identifier 10.1109/JMEMS.2008.922079

charged particles into ordered lattices and 2) adhering charged particles to a substrate bearing a spatially resolved pattern of complementary charge. In the absence of an applied electric field, charged colloids assemble into aggregates with minimal order [17]–[19], and mesoscale spheres assemble into a limited array of 2-D lattices [20]. Recently, Kalsin *et al.* [21], [22] demonstrated that a binary mixture of colloids with opposite charges can crystallize into well-ordered, nonclosed packed, or core-shell structures by controlling the ratio of particles in solution. In an external electric field, extended lattices with controlled morphology are possible [23]–[25].

When a substrate bears a pattern of charge, particles with the opposite charge will tend to adhere to the charged regions. Potential applications of such materials include the creation of chemical or biological sensors [26]–[28]. Although particles are typically deposited from liquid suspension, they may also be deposited from the gas phase [29]. As part of a growing interest in using xerographylike processes to pattern nanostructures, "toner" particles have been patterned into ~60-nm-wide lines [30].

Templated Electrodes for High-Voltage Self-Assembly: We have previously described a technique in which a high-voltage dc bias applied to a patterned gold electrode on a polystyrene substrate assembled 100-μm-diameter glass spheres into arbitrary patterns and lattices, with one sphere per window [1]. These patterns of microspheres were transferred into other substrates (e.g., polydimethylsiloxane (PDMS) or epoxy). Here, we explore the generality and scope of this technique, demonstrate the range of materials that can be used for the substrate, electrode, and particles, and compare our experimental observations directly to the predictions made by the theoretical model that we have developed and by subsequent finite-element calculations. We also determine the size of the particles that can be assembled and demonstrate assemblies with multiple particles per window.

II. Results and Discussion

Experimental Design: In detail, the general scheme for self-assembly has been previously described [1]. Our goal within this paper is to investigate the scope and importance of each parameter in this system and determine their effect on the yield of the assemblies. Here, we provide a brief review of the process. First, an ~50-nm conductive film was evaporated onto a dielectric substrate. In most cases, this conductive film was a coinage metal that was patterned by microcontact printing using 1-hexadecanethiol and subsequently etched to reveal windows in the metal by exposing the underlying dielectric substrate [31]. After pouring several layers of dry particles over the patterned electrode, a dc voltage (10–20 kV) between the electrode and a grounded plate positioned beneath the substrate was applied for 2–5 s. When subjected to gentle manual agitation while applying the dc bias, the particles assembled into an array in which there was one particle over each window; no particles were observed over the continuous region of the electrode. The mechanical agitation was applied by tapping the substrate at a rate of ~1 Hz in which the extent of the agitation was determined optically to ensure that sufficient agitation removed excess spheres but not such that it was too violent to remove correctly positioned particles. This general procedure was used for the experiments in this paper, except where otherwise noted.

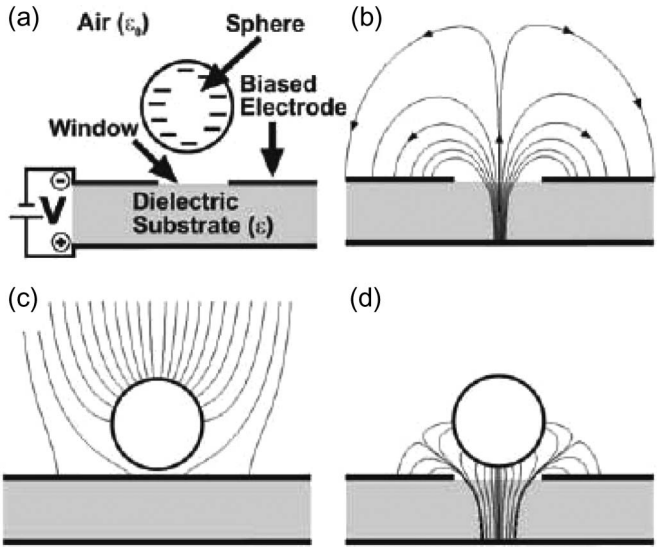

Fig. 1. (a) Schematic illustration describing the unit cell of our experimental setup used for the finite-element calculations of the electric field lines. A unit cell includes a single window with the biased and lower electrode present. We illustrate the electric field under the following three conditions: (b) No sphere present; (c) a charged sphere over the biased electrode; and (d) a charged sphere over a region of a window. The field in (c) illustrates a repulsive force between the charged sphere and the upper biased electrode. In (d), the field shows an attractive force between the charged sphere and the lower electrode.

Mechanism of Assembly: A detailed description and calculation of the forces that control the process of assembly are published elsewhere [2]. Here, we provide a brief outline of the mechanism as motivation for the particular experiments that we chose to perform. Fig. 1(a) shows a schematic of the components used in the calculation of the electric field. The spherical particles become charged, with the same sign as the biased electrode, presumably by some combination of direct charge transfer and corona charging (it will be shown that the electric field near the particle is sufficient to create corona discharge). Fig. 1(b) shows the electric field created by a biased patterned electrode with an oppositely charged grounded electrode beneath. Fig. 1(c) and (d) shows the electric field around a charged sphere positioned over the biased electrode and over a window, respectively. A particle that is located above the biased electrode will experience an upward force because it is repelled from the electrode bearing a charge of the same sign; this electrostatic force on a charged sphere scales as

$$F_{\text{rep}} \sim \varepsilon_0 (U/L)^2 D^2 \tag{1}$$

where ε_0 is the permittivity of free space, U is the applied potential, L is the size of the patterned electrode, and D is the diameter of the sphere. This particle needs to be expelled from the surface during assembly, and the repulsive electrostatic force must exceed the force of gravity on the particle. This criterion establishes a minimum voltage that must be applied in order to eject a sphere from the surface

$$U_{\min} \sim L(D\rho g/\varepsilon_0)^{1/2} \tag{2}$$

TABLE I
MEDIAN OPTIMIZED YIELD[a] FOR THE SELF-ASSEMBLY OF BEADS ON PATTERNED ELECTRODES: EFFECTS OF BEAD SIZE, GEOMETRY, AND MATERIALS

bead material	electrode material	dielectric material	bead diameter (μm)	ratio of window size to bead size	median optimized yield (%)
glass	gold	PS	20	1 : 1.3	91
glass	gold	PS	75	1 : 1.1	97
glass	gold	PS	100	1 : 1.4	98
glass	gold	PS	200	1 : 1.0	> 99
glass	gold	PS	280	1 : 1.4	98
glass	gold	PS	650	1 : 1.3	94
glass	gold	PS	750	1 : 1.5	91
glass	gold	PS	100	1 : 0.9	< 70
glass	gold	PS	100	1 : 1.0	97
glass	gold	PS	100	1 : 1.4	98
glass	gold	PS	200	1 : 1.0	> 99
glass	gold	PS	200	1 : 2.0	98
glass	gold	PS	200	1 : 3.0	87
glass	gold	PS	200	1 : 4.0	< 75
PS	gold	PS	100	1 : 1.4	99
copper	gold	PS	40	1 : 1.3	96
silicon	gold	PS	*ca.* 100	*ca.* 1 : 1.4	98
glass	gold	SU-8[b]	100	1 : 1.4	99
glass	gold	PDMS	100	1 : 1.4	99
glass	copper	PS	100	1 : 1.4	95
glass	silver	PS	100	1 : 1.4	97

[a] Median percent yield (as defined in the text) calculated for repeated experiments under optimized conditions. Yields in such repeated experiments varied by no more than 1-2%.

[b] 25-μm film on a conductive (p-type) silicon wafer.

where ρ is the density of the sphere and g is the acceleration due to gravity. We have previously shown that (2) is valid for our system and that the ratio of $U_{\min}$ for two different types of beads—copper shot and glass spheres—is equivalent to the ratio of the square root of the product of the diameter and density of the particles, as predicted.

A particle that is situated over a window will experience a downward attractive force to the oppositely charged grounded electrode below the window. This attractive electrostatic force is proportional to the attractive force on a small circular region of an ideal parallel-plate capacitor

$$F_{\text{att}} \sim \varepsilon (U/t)^2 d^2 \tag{3}$$

where ε is the permittivity of the dielectric substrate, U is the applied potential, t is the thickness of the dielectric substrate, and d is the diameter of the circular window. In order for the particle to remain over the window, the attractive force must prevent the particle from rolling or sliding off the window during agitation. As discussed in the paper describing the theory behind this technique [2], both repulsive and attractive forces depend on the geometry of the system and on the applied voltage. There are some parameters that do not appear in any of the equations for the theory—most notably the dielectric constant of the particles. Here, the experimental constraints on both the geometry and the materials used in this system are explored, and these results are compared to the theoretical predictions; also, this technique was expanded to illustrate its usefulness and the range of its capabilities.

Evaluating the Success of This Assembly Process: This method of templated self-assembly did not yield perfect arrays. Equation (4) defines the defect rate of our assemblies

$$\% \text{ Defects} = (n/s) * 100 \tag{4}$$

in which n is the number of defects and s is the number of sites. A "defect" is either an extra sphere in an unwanted location or a sphere missing from a desired site. We define the percent yield of an assembly as 100% minus the defect rate. Table I provides an overview of our results, reported as median yields for repeated experiments under optimized conditions. The experimental parameters that were optimized were the length of time that the high voltage was applied and the amount of agitation that was required. The yield of the assemblies was not affected by the voltage applied to the electrode as long as it was greater than the minimum voltage (2) needed to eject spheres and less than the dielectric breakdown of air or of the substrate. In cases when the voltage was too small or too great, no assembly was observed (Fig. 2).

Yields in excess of 97% were often achieved for a wide range of sizes of beads, materials, and ratios of window size to bead size. Each of these constraints was considered with respect to predictions from our model in the discussion that follows.

A. Geometric Constraints

Limitations on the Diameter of the Sphere: Our model suggests that there is an upper bound to the size of the sphere that could be assembled. The upper limit is determined by the

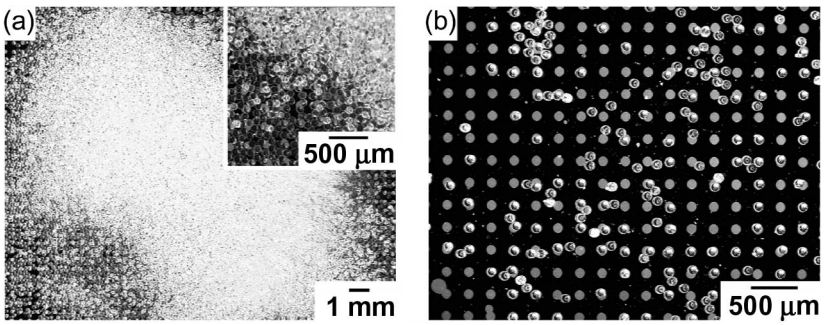

Fig. 2. Optical images of control experiments that do not yield assembled particles. (a) Using a voltage that is not sufficient for lifting (in this case, ∼2 kV), all the spheres remain on the surface of the electrode, and none is ejected. (b) Applying 30 kV (a voltage that is great enough to cause dielectric breakdown of air) to a similar electrode results in all the spheres being ejected from the system during the breakdown event.

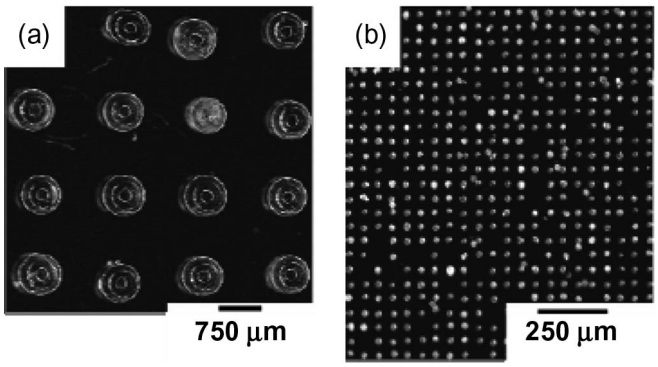

Fig. 3. Optical images of glass microspheres with the smallest and largest diameters that assemble with minimal defects. (a) An array of 750-μm-diameter spheres in a square lattice that assembled over 500-μm-diameter circular windows with a pitch of 1.5 mm, using an applied potential of -20 kV (100% yield). (b) The 20-μm-diameter spheres assembled over 15-μm windows with a pitch of 50 μm, using an applied voltage of -20 kV (91% yield). The major source of error is vacant windows, which, we believe, is due to the clustering of spheres.

minimum voltage (2) needed to eject a sphere. This voltage must not lead to the dielectric breakdown of the surrounding gas. This breakdown voltage, as explained by Paschen's law $(V = f(p, d))$, is a nonlinear function that is dependent on the pressure of the gas (p) and the gap between electrodes (d) [32]. It is also known to depend on the type of gas and the geometry of the electrodes. In our case and for the purposes of discussion within this paper, we refer to the specific case of ambient conditions at 1 atm where the breakdown of air is ∼30 kV/cm.

As previously reported, $U_{\min}$ for ejecting for a glass sphere ($\rho = 2.44 \times 10^3$ kg/m^3) with a diameter of 100 μm is ∼10 kV. The theory predicts that the voltage required to eject a particle is proportional to the square root of the diameter. For a glass particle, the maximum size that could be ejected at 30 kV is ∼900 μm. Glass spheres as large as 750 μm successfully assembled [Fig. 3(a)], but 1-mm spheres were too heavy to be ejected from the patterned electrode using this maximum applied bias. Because the experimental results very closely equal those predicted by the theory of (2), it was determined that the missing coefficient from (2) required for equality is approximately one. The maximum potential that our experimental setup can achieve is ∼30 kV because the setup is current limited; the leads from the electrode are able to ionize the air, which creates a current and prevents higher potentials from being obtained.

There is no intrinsic lower limit on the diameter of the sphere imposed by our model. Our model is simple and only includes electrostatic and gravitational forces, the two most significant forces in our system for mesoscale objects. Because this system assembles dry particles, other forces—most specifically adhesion and van der Waals forces—become comparable with gravitational forces as particles become smaller. Stiction is a known problem in MEMS devices and in any dry component system when components become small; these forces set the lower bound on the diameter of spheres that could be assembled with this technique.

The theory of Johnson *et al.* [33] describes the adhesive forces between macroscopic objects. The minimum force required to separate two spheres that are in adhesive contact is given by

$$F = -\frac{3\pi}{2}\gamma_{12}\frac{R_1 R_2}{R_1 + R_2}. \tag{5}$$

In this equation, γ_{12} gives the interfacial free energy between the two materials (the work of adhesion), and R_1 and R_2 are the radii of the spheres. For adhesion between a sphere with radius R_1 and a flat plane, one would ideally set R_2 to infinity. For surfaces that are not atomically smooth, however, one should set R_2 equal to the average radius of the asperities on the surface [34]. To obtain an order-of-magnitude estimate of these adhesive forces, we assume that the asperities have a radius of ∼1 nm and that the work of adhesion is on the order of 100 mN/m. The adhesive force estimated from (5) is roughly 10^{-10} N for any sphere that is much larger than the radius of the asperities (the mathematical form of the equation makes the radius of the larger sphere irrelevant). This force is equal to the gravitational force on a glass sphere with a diameter of ∼20 μm. This rough estimate agrees with the general observation that adhesive forces are greater than gravitational forces for objects with diameters of ∼10μm and less [35].

Glass spheres as small 20 μm in diameter successfully assembled [Fig. 3(b)]. It is extremely difficult to obtain dry particles of 10 μm or smaller in diameter that do not tend to cluster together [35]. Clusters of particles are ejected as a single entity and leave numbers of adjacent windows vacant. Additionally, nonspecific adhesion between individual particles

and the electrode caused excess spheres to remain. We believe that this lower size limit would apply generally to the self-assembly of small particles under dry conditions.

Limitations on the Ratio Between the Diameters of the Windows and Spheres: In order for self-assembly to be a useful method of fabrication, the resultant structures must be nearly defect free. Our system is modeled as a parallel-plate capacitor in which the upper patterned electrode contains windows. The assembly proceeds under an applied bias by attracting charged particles over the windows, which lowers the total energy of the capacitor; ideally, these particles cover as much of the window as possible. The introduction of dry particles to the system by pouring multilayers of spheres over the patterned electrode is a stochastic process in which the distance between a window and the nearest bead is determined by the ratio of the diameter of the window to the diameter of the bead. This ratio will determine the probability for achieving assemblies with high yield.

The force between a bead and a vacant window is always attractive, but it decays rapidly as the distance between the sphere and the center of the window increases [2]. In the limit where a sphere is far from a window, the force between a charged sphere and the upper electrode is repulsive. Using a 2-D finite-element calculation, the vertical force on a cylinder that was adjacent to a window was computed. Both the size of the cylinder (D) and the distance between the center of the cylinder and the center of the window (x) were held constant; the diameter of the window (d) was varied. These computations showed that the attractive (vertical) electrostatic force equals zero when the ratio of d/D was 0.45 (Fig. 4). Because the gravitational force is relatively small at these size scales, when the ratio was decreased further, the electrostatic force became great enough to eject a sphere from the system. These calculations represent a case in which a bead would adhere to a window and assemble correctly despite initially not residing over a window.

Because the spheres are added dry to the system and pack under gravitational forces, they most likely form a disordered hexagonally closed-packed or face-centered cubic lattice structure [36]. If a window does not have a bead directly above it, the lateral force (calculated earlier) pulls the nearest bead toward that window. When the windows are significantly smaller than the beads, it is unlikely that each window will end up with a bead directly over it; rather, the distribution of distances between spheres and windows would be random. Experimentally, successful assembly when the ratio of the diameter of the window:bead was $1:3$ was observed [Fig. 5(a)]. If the ratio was less than $1:3$, many of the windows were vacant. The yield was only 75% when the ratio of the diameter of the window to the diameter of the sphere was $1:4$ [Fig. 5(b)]. The experimental results permit a smaller ratio than the predicted model (a ratio of 0.33 versus 0.45, respectively), and these experimental results demonstrate the point at which the probability becomes significant that no sphere is initially positioned close enough to a window to be attracted to that windows.

At the other limit in which a window is too large, defects will arise from multiple spheres assembling over a single window. Experimentally, a successful assembly could be achieved if the diameter of the window and the diameter of the bead were of equal size (ratio of $1:1$) [Fig. 5(c)]. At a ratio that is greater than $1:1$, it is geometrically possible for two or more spheres to contact a single window. Two spheres contacting a single window provide a greater coverage of the upper electrode than a single

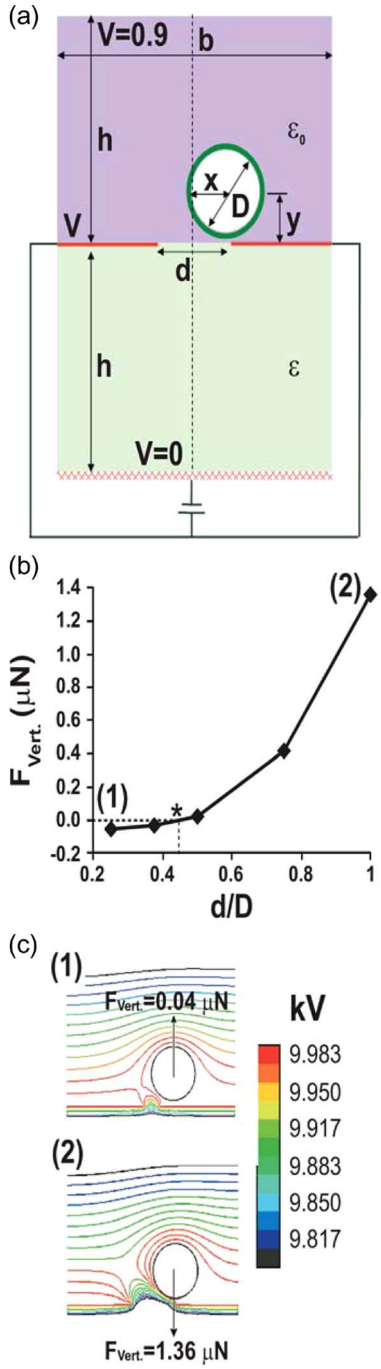

Fig. 4. (a) Schematic of the unit cell used for the 2-D finite-element-method calculation. The parameters of the calculation were $V = 10$ kV, $d = 100$ μm, $h/d = 10$, $\varepsilon/\varepsilon_0 = 2.6$, $b/d = 4$, and $y/d = 0.6$; the out-of-plane length of the cylinder $L_0/D = 1$. The parameter (d/D) was changed to determine the point at which the vertical force changed sign. (b) A graph of the vertical component of the electrostatic force on the cylinder. A positive force is in the downward direction (attraction between the cylinder and the substrate). The vertical force is zero (represented by an $*$ on the graph) at a ratio of $d/D = 0.45$. (c) Graphical representations of the equipotential lines for two of the points labeled (1) and (2), respectively, in (b). In (1), the calculated electrostatic force is repulsive, whereas in (2), the electrostatic force is attractive to the window.

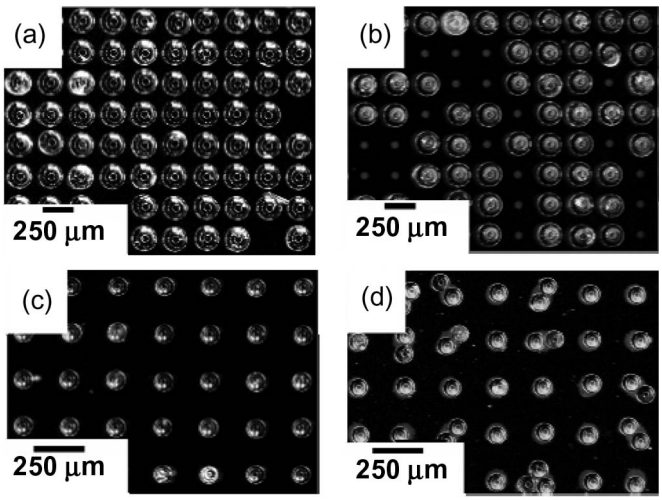

Fig. 5. Optical images of assemblies of spheres with different ratios of the diameter of the PS window to the diameter of the assembled microspheres. The upper and lower ratios for which we were able to achieve successful assemblies of a single sphere over each window are shown. (a) Successful assembly occurred when spheres that were 200 μm in diameter assembled over windows with a diameter of 67 μm (ratio of 1 : 3) and a pitch of 250 μm (96% yield). (b) Many windows were vacant when we tried to assemble spheres with a diameter of 200 μm over windows with a diameter of 50 μm (ratio of 1 : 4) and a pitch of 250 μm (72% yield). (c) Highly ordered assemblies resulted from 100-μm-diameter spheres over 100-μm-diameter windows (ratio of 1 : 1) with a pitch of 250 μm (100% yield). (d) Multiple spheres (doublets and triplets) assembled over single windows when 100-μm-diameter spheres were assembled over 110-μm-diameter windows (ratio of 1.1 : 1) with a pitch of 250 μm (68% yield).

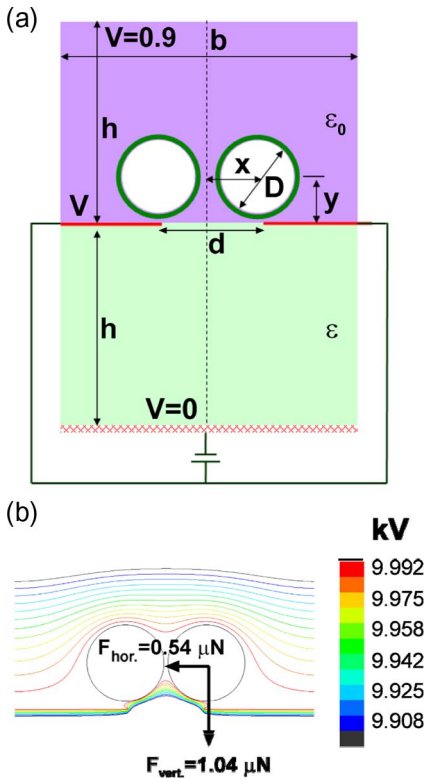

Fig. 6. (a) Schematic of the unit cell used for the 2-D finite-element-method calculation. The parameters of the calculation were $V = 10$ kV, $d = 100$ μm, $h/d = 10$, $\varepsilon/\varepsilon_0 = 2.6$, $D/d = 1$, $b/d = 4$, and $x/d = 0.525$; the out-of-plane length of the cylinder $L_0/D = 1$. (b) A graphical representation of the equipotential lines for two cylinders residing over the edge of a window. The observed net force is down toward the lower plate and toward the center axis of the window; the two cylinders are attracted toward the center of the window despite having the same charge.

sphere positioned at the center of the window, but because both spheres are charged, they are repelled from one another. Using a 2-D finite-element calculation, the net horizontal force on each of the two identical cylinders that were adjacent to a window was computed. With both similarly charged cylinders residing over the edge of the electrode, the two cylinders were attracted to each other; the electrostatic force toward the center axis of the window due to the lower electrode was greater than the repulsive force between the two similarly charged cylinders (Fig. 6). In the simplified 2-D calculation in which the size of the window equaled the diameter of the cylinder, both cylinders were attracted to the window. In the 3-D experiment, multiple beads assembling over a single window were only observed when the ratio of the diameter of the window to that of the sphere was greater than one. With a ratio of 1 : 0.9, ~25% of the windows were covered by two spheres; a few windows had three spheres [Fig. 5(d)].

Although a wide range of ratios—from 1 : 1 to 1 : 3—yielded successful results, the optimal ratio for high-yield assemblies was found to be approximately 1 : 1.5. This ratio best compensates for polydispersity in the sizes of the beads and the sizes of the windows.

Limitations on Multiple Beads Packing Into Large Windows: As previously discussed, if the size of a window is greater than the size of a sphere, multiple spheres will assemble to maximize the coverage over a single window in order to minimize the energy of the system. By fabricating windows with geometries that are larger than a single sphere and in noncircular geometries, it is possible to extend this technique to assemble arrays of higher order structures containing multiple spheres per window. Fig. 7 shows examples of multiple beads assembling over large windows. Arrays of ordered clusters of beads, with three beads over each triangular window when the length of the side of a triangle was 1.4-times the diameter of a sphere, were successfully assembled [Fig. 7(a)]. The geometry of the windows on the patterned electrode determined the orientation of the array of spheres. Windows in the shape of a ring guided the spheres to assemble into rings one particle wide, although the interparticle spacing was not well controlled [Fig. 7(b)]; each ring contained approximately 20 spheres. Large numbers of spheres also assembled over windows of arbitrary shape [illustrated by Arabic numerals, Fig. 7(c)]. The spheres always appeared to maximize the coverage over each window, as predicted by the model of a parallel-plate capacitor.

B. Material Constraints

Range of Materials That Can Be Assembled: Our theory assumes that the assembled particles are charged to an equipotential surface with that of the electrode, either by electron conduction between the electrode and the particle or by ionic/corona charging of the air by the metal edges along the patterned electrode. Because this process is dry, a pile of metallic or semiconducting particles in contact with the biased

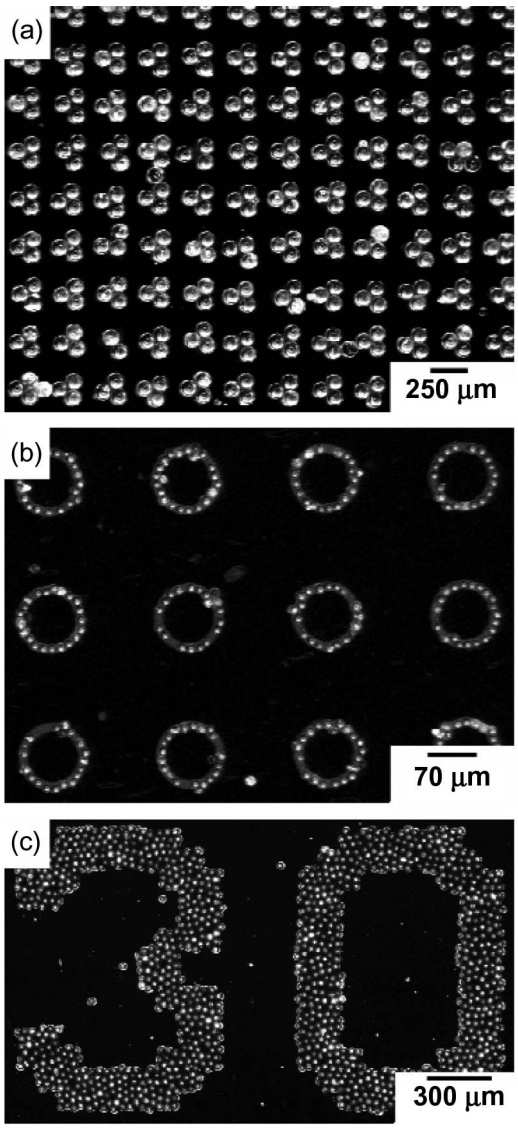

Fig. 7. Multiple beads assemble over single windows into the desired structures. (a) Assembly of 100-μm-diameter glass spheres over triangular windows with an edge length of 140 μm results in an array with three spheres per window. (b) Assembly of 20-μm-diameter glass spheres over annular windows results in an array of rings of spheres. (c) Assembly of 40-μm-diameter copper shot over large windows (Arabic numerals) results in approximately close-packed coverage of the windows by the spheres.

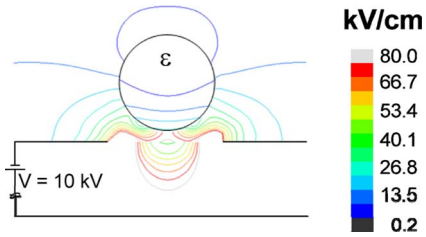

Fig. 8. Graphical representation from a 3-D finite-element-method calculation of the magnitude of the electric field between a sphere residing over the axis of a window and the edge of the biased electrode. The parameters for this calculation were an applied voltage of 10 kV, both the diameters of the sphere and window that were 100 μm, and the dielectric constant of the sphere (ε) of the sphere that was 2.6 (the dielectric constant of polystyrene which has the smallest ε of all the materials that we assembled).

patterned electrode most likely charges by electron conduction. For insulators—glasses and polymers—the mechanism of charging is less obvious. Using a 3-D spherical symmetry calculation, the initial electric field between a sphere over the axis of the window and the upper biased electrode was determined. In all previous calculations, the sphere was set to have an equipotential surface with the biased electrode, but in this calculation, the sphere was set to be uncharged. The calculated electric field in the gap between a sphere aligned with the axis of a window and the edge of the upper biased (10 kV) electrode was 80 kV/cm, and a maximum electric field, which was $\sim$10 μm from the tip of the electrode, was 100 kV/cm (Fig. 8). These calculations of the electric field and volume of space between the sphere and the electrode are great enough to cause dielectric breakdown of the surrounding gas (electric fields that are $>$ 30 kV/cm are capable of breakdown of air at 1 atm) [32] and create a corona (gaseous ions) that provides a conductive path between the electrode and the spheres and could charge the spheres.

Neither the repulsive force (2) nor the attractive force (3) includes a term for either the dielectric constant or any other intrinsic property of the sphere. If this assumption is valid, there are no limitations to the type of material that can be assembled using this technique, as the forces act equally on conductive and insulating materials and should therefore have similar yields. Fig. 9 shows the full spectrum of bulk electrical properties of the particles that can be successfully assembled: insulators (polystyrene), semiconductors (silicon particles), and conductors (copper shot). For simplicity, our theory uses spherical particles in all of the equations and calculations, but there is no fundamental limitation on the geometry of the particle. In Fig. 9(b), the silicon particles are irregular in shape; this observation demonstrates that nonspherical and nonsymmetric particles assemble.

Range of Materials That Can Be Used as the Dielectric Substrate: The theory includes both the material and thickness of the dielectric substrate as parameters. The attractive force (3) is linearly proportional to the permittivity of the substrate (ε) and inversely proportional to the square of the thickness ($1/t^2$). These proportionalities suggest that thinner substrates of materials with a large permittivity would be ideal in order to maximize the attractive force and minimize defects due to excessive agitation or further processing of the assembled spheres.

There is a lower limit imposed on the thickness of this dielectric substrate. The maximum applied voltage is constrained by the following two conditions: 1) $U < U_{\text{air breakdown}}$; the voltage is limited by the dielectric breakdown of gases present (ca. 30 kV for our experimental setup, as discussed earlier). 2) $U < t^* E_{\text{die}}$, where E_{die} is the dielectric strength of the substrate (the electric field above which dielectric breakdown occurs). Zhu *et al.* [2] showed that the minimum voltage for assembly is determined by setting the gravitational force on a bead equal to the repulsive electrostatic force (1) to determine the minimum required voltage to eject a sphere. From our previous results, it was determined that the coefficient for the electrostatic forces is approximately one; if the voltage is substituted as limited in the second case into (2), a solution for

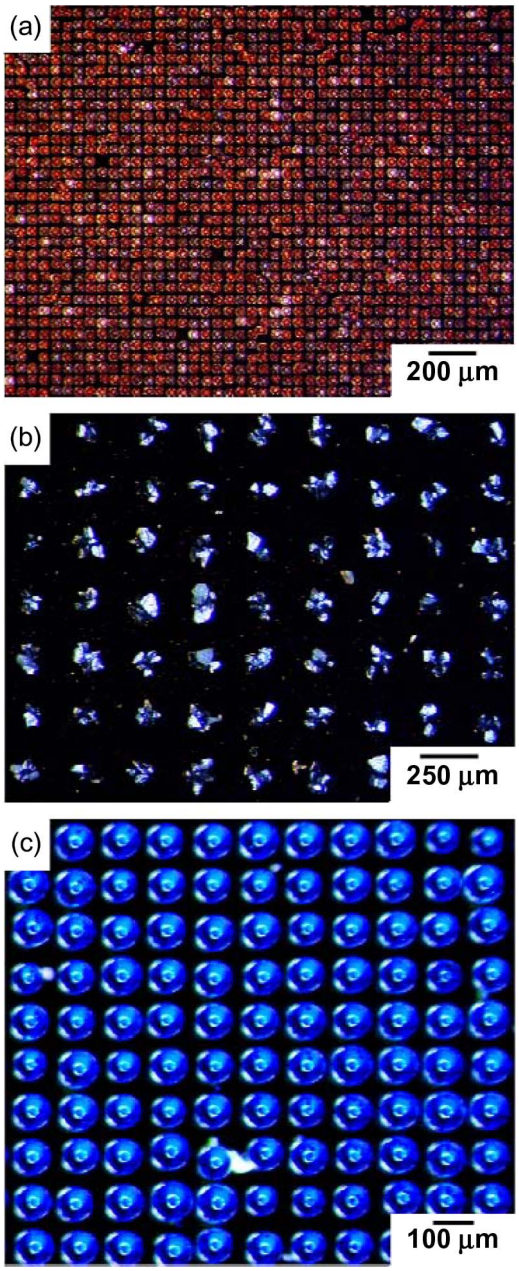

Fig. 9. Optical images of successful assemblies of a variety of materials with a wide range of electrical properties. (a) A square array of 40-μm-diameter copper shot successfully assembled (98% yield). (b) An array of silicon powder (90–106 μm in diameter) assembled into a square lattice (97% yield). This image illustrates that nonspherical particles can also assemble by this method, with one particle per window. (c) A lattice of blue-dyed polystyrene spheres (100-μm diameter dyed with 1,4-bis(pentylamino)anthraquinone) self-assembled over PS windows (100% yield).

the minimum thickness of the substrate necessary to achieve a successful assembly is obtained as

$$t_{\min} = L(D\rho g/\varepsilon_0)^{1/2}/U_{\text{die}}. \tag{6}$$

The case of a 100-μm glass particle on a 10-mm electrode with a dielectric substrate ($U_{\text{die}} \sim 10^8$ V/m), [37] yields a minimum thickness of 50 μm. The thinnest substrate that experimentally produced a successful assembly was a 25-μm film of epoxy on a silicon wafer; with this substrate, a voltage of $\sim$5 kV was applied.

As expected, when a noninsulating substrate (e.g., a silicon wafer or an aluminum plate) that has a very large permittivity was tried, no assemblies were observed as no potential difference could be established between the upper biased electrode and the lower grounded electrode.

The substrate must also maintain the voltage on the patterned electrode and prevent current from leaking along the surface to ground. The leakage of current is a function of the surface conductivity and the shortest distance along the surface from the biased electrode to ground. Polymers such as 1-mm-thick polystyrene Petri dishes with 35-mm diameter and 3-mm-thick sheets of PMMA, 4 cm $\times$ 4 cm, were convenient substrates for assembly. All surface resistivity measurements were done following the protocol per ESD S11.11. The surfaces were all exposed to an environment of 12% relative humidity at 73 °F for 48 h before testing. Measurements were obtained at either 100 or 500 V. The surface resistivity of the polystyrene was measured to be greater than 2×10^{15} Ω/square (beyond the limit of detection); a literature value is 3×10^{16} Ω/square [38]. Also, successful assemblies were achieved on 75-mm-diameter alkali-free glass wafers that had a surface resistivity that was greater than 2×10^{15} Ω/square. Conversely, successful assemblies were not able to be achieved using standard glass microscope slides (Type II soda–lime glass, 50 mm $\times$ 75 mm). Corona discharge from the edges of the slides and occasional electrostatic discharge due to the electrical breakdown of air were observed. The surface resistivity of these substrates was measured to be only 1.40×10^{13} Ω/square, at least 100-times smaller than that of the alkali-free glass; this result suggests that a substrate that is at least 100-times larger on each side would be necessary for a successful assembly. After modifying the surface of the soda–lime glass with a fluorosilane (tridecafluoro-1,1,2,2-tetrahydrooctyl-1-trichlorosilane), successful assemblies were still unable to be achieved. Although the surface resistivity of the fluorinated soda–lime glass (2.11×10^{13} Ω/square) was greater than that of the native surface, it was still approximately two orders of magnitude less than that of the substrates that yielded successful assemblies. In addition, the ambient humidity affects the surface conductivity; an increase in humidity causes the conductivity to increase. When the relative humidity was above 65%, it was not possible to produce assemblies on any of the glass substrates (alkali-free, soda–lime, or fluorinated soda–lime glass).

Assemblies over flexible substrates are of interest for producing flexible electronics. Successful assembly was achieved over a flexible polymer substrate, a film of PDMS that is approximately 1 mm thick. Gold films evaporated onto the PDMS buckle and crack due to thermal expansion of the PDMS during evaporation and subsequent flexing of the substrate [39]. Although both buckling and cracking were present in our patterned electrode on the PDMS substrate, neither adversely affected the quality of the assembly (Fig. 10).

Range of Materials That Can Be Used as the Patterned Electrode: Our model does not include any parameters regarding the choice of material for the patterned electrode; this

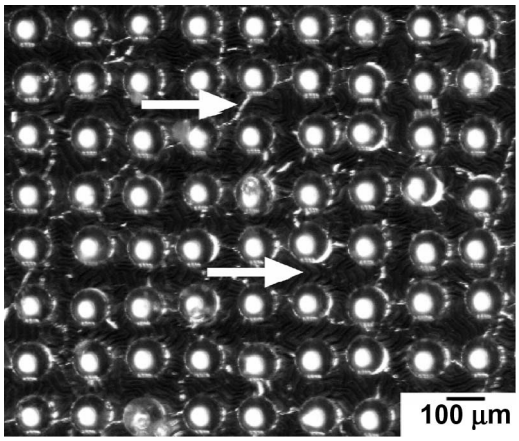

Fig. 10. Optical image of an assembly of 100-μm-diameter glass spheres over a flexible PDMS substrate that supports a gold electrode (100% yield). The spheres yield a successful assembly despite the gold electrode having (noted by arrows) minor defects, such as (white lines) cracks due to flexing of the substrate and (dark lines) buckling occurring during the metal deposition process.

observation suggests that any material that is capable of patterning should suffice. The only technical prerequisite for a material to serve successfully as an electrode in our system is that it must be able to achieve and maintain an equipotential surface across the entire electrode at the desired potential. Patterned electrodes were able to be fabricated, and successful assembles could be obtained with all coinage metals (Au, Ag, and Cu). These electrodes were fabricated by evaporating a thin film of metal using an electron-beam evaporator. Subsequently, the metal film was patterned with an alkanethiol resist by microcontact printing using PDMS stamps [31] and etched with an appropriate solution to reveal the desired patterned electrode [40], [41]. In addition to the coinage metals, arrays were successfully assembled over a patterned electrode consisting of amorphous silicon. The silicon film was more difficult to pattern than the coinage metals. It required additional lithography, deposition of a sacrificial metal layer, liftoff, and etching to obtain a patterned silicon electrode. The silicon electrode could only be patterned on a glass substrate, not on a polymer substrate, in order to accomplish successfully every step of the process.

III. Conclusion

We have explored the self-assembly of micrometer-sized particles using a patterned electrode on a dielectric substrate with an applied electric field. We have experimentally verified the following: 1) the limitations on the size of particles for this method of self-assembly; 2) the ability for a wide range of materials (dielectrics, semiconductors, and metallic particles) and sizes to be patterned over a diverse set of substrates; and 3) the scope and limitations of our theoretical model.

Electrostatic self-assembly has several useful characteristics. It is applicable to a greater range of materials, substrates, and patterns than most other techniques of self-assembly. The geometric constraints on this system are minimal: 1) It can assemble glass spheres over a wide range of sizes (20–750 μm); 2) it produces assemblies in high yield over a large range of ratios between the diameter of the sphere and the diameter of the window; evidence suggests an optimal ratio of approximately 1 : 1.5; and 3) it can generate higher order structures such as arrays of ordered clusters of particles.

The choice of materials does not appear to constrain the system: 1) The technique can assemble particles with any bulk electrical property (metal, semiconductor, or insulator); 2) the electrode can be made of any coinage metal or conductive material that can be appropriately patterned; and 3) the dielectric substrate must prevent electrical conductivity through its bulk and along its surface in order to maintain the bias applied to the patterned electrode.

This process of self-assembly has the following several disadvantages: 1) The most important limitation is that the system is sensitive to adhesion and does not work well with objects that are smaller than $\sim$20μm; 2) each system is limited to a single type of particle; there is no selectivity in this assembly process; 3) this technique is limited to 2-D patterns; and 4) the high voltages used in this process could damage components that are sensitive to electrostatic discharge.

IV. Experimental Section

All materials and chemicals were purchased and used as received. The fabrication of the patterned gold electrodes on a polystyrene substrate and the method for self-assembly of glass spheres were identical to our previous communication [1] (warning: use caution when handling these large voltages). Hereafter, we will describe all deviations from that experimental procedure for the assemblies using different materials for the particles, substrates, and electrodes.

Particles: The fabrication of the electrodes and the process for assembly did not differ for any of the particles. The assembly of the glass and polystyrene microspheres (Duke Scientific), silicon powder (Glen Mills, Inc.), and copper shot (ACuPowder International, LLC) followed the previously reported procedures.

Substrates: The PMMA sheet (Small Parts, Inc.), along with both the standard glass slides (Type II soda–lime glass, Corning Inc.), and the alkali-free glass wafers (Plan Optik) were treated similarly to the polystyrene (PS) substrates. The SU-8 (MicroChem Corporation) was spin coated onto a gold-coated alkali-free glass wafer. The entire wafer was exposed to UV light (AB-M mask aligner) to cross-link the polymer yielding a thin film with a thickness of 25 μm. The gold film on the glass wafer was the ground electrode during the assembly. For the PDMS substrate, the prepolymer was spin coated onto a glass slide, cured at 70 °C for 1 h, and oxidized in an air plasma cleaner for 1 min. Positive photoresist was spin coated onto the PDMS substrate and patterned by exposing the resist to UV light through a photomask with the desired electrode design. We evaporated a chromium adhesion layer and a gold film using an electron-beam evaporator at a rate of 1 nm/s to try and minimize the amount of buckling in the film. Washing the substrate in acetone removed the remaining photoresist and lifted off the undesired metal revealing the gold electrode on the PDMS substrate. The substrate was dried in an oven for 10 min at 70 °C to remove any excess solvent.

Electrodes: The electrodes were deposited using an electron-beam evaporator onto the desired substrate. The coinage metals

(Au, Ag, and Cu) were deposited on PS substrates and patterned with 1-hexadecanethiol using an appropriate PDMS stamp. Only the gold required an adhesion layer of Cr. The unpatterned regions of the gold and silver films were selectively etched by a solution of 1-M KOH, 0.1-M $Na_2S_2O_3$, 0.01-M $K_3Fe(CN)_6$, and 0.001-M $K_4Fe(CN)_6$. An acidic solution of 0.012-M $FeCl_3$ etched the bare copper regions.

The silicon electrode required a multistep fabrication process. First, amorphous silicon was evaporated onto an alkali-free glass wafer. A positive photoresist (Rohm and Haas) was spin coated over the silicon film. By using a photomask and a UV mask aligner (ABM), the photoresist was patterned with the pattern of the electrode. After developing the photoresist to reveal the silicon substrate below, a layer of copper was deposited as a resist for the revealed silicon. The remaining photoresist was removed by washing with acetone. A solution of KOH in water and ethanol at 70 °C etched the unprotected silicon, revealing the patterned silicon electrode covered with copper. The aqueous $FeCl_3$ solution etched the copper, leaving only the patterned silicon electrode on the glass wafer.

Surface Resistivity: All surface resistivity measurements were done following the protocol per ESD S11.11 by Fowler Associates, Inc. (Moore, SC).

Theoretical Computations: The distribution of electric field was analyzed by using the finite-element program ABAQUS (ABAQUS, Reference Manuals, 2005. Hibbit, Karlsson and Sorenson, Inc., Pawtucket, RI). The force on the bead was calculated by integrating the Maxwell stress acting on the surface of the bead [2].

REFERENCES

[1] A. Winkleman, B. D. Gates, L. S. McCarty, and G. M. Whitesides, "Directed self-assembly of spherical particles on patterned electrodes by an applied electric field," *Adv. Mater.*, vol. 17, no. 12, pp. 1507–1511, 2005.

[2] T. Zhu, Z. G. Suo, A. Winkleman, and G. M. Whitesides, "Mechanics of a process to assemble microspheres on a patterned electrode," *Appl. Phys. Lett.*, vol. 88, no. 14, p. 144 101, Apr. 2006.

[3] B. A. Parviz, D. Ryan, and G. M. Whitesides, "Using self-assembly for the fabrication of nano-scale electronic and photonic devices," *IEEE Trans. Adv. Packag.*, vol. 26, no. 3, pp. 233–241, Aug. 2003.

[4] C. J. Morris, S. A. Stauth, and B. A. Parviz, "Self-assembly for microscale and nanoscale packaging: Steps toward self-packaging," *IEEE Trans. Adv. Packag.*, vol. 28, no. 4, pp. 600–611, Nov. 2005.

[5] R. R. Tummala, Ed., *Fundamentals of Microsystems Packaging*. New York: McGraw-Hill, 2001.

[6] M. Boncheva and G. M. Whitesides, "Making things by self-assembly," *MRS Bull.*, vol. 30, no. 10, pp. 736–742, Oct. 2005.

[7] G. M. Whitesides and B. Grzybowski, "Self-assembly at all scales," *Science*, vol. 295, no. 5564, pp. 2418–2421, Mar. 2002.

[8] S. A. Stauth and B. A. Parviz, "Self-assembled single-crystal silicon circuits on plastic," *Proc. Nat. Acad. Sci. U.S.A.*, vol. 103, no. 38, pp. 13 922–13 927, Sep. 2006.

[9] H. J. J. Yeh and J. S. Smith, "Fluidic self-assembly for the integration of GaAs light-emitting diodes on Si substrates," *IEEE Photon. Technol. Lett.*, vol. 6, no. 6, pp. 706–708, Jun. 1994.

[10] D. A. Bruzewicz, M. Boncheva, A. Winkleman, J. M. St Clair, G. S. Engel, and G. M. Whitesides, "Biomimetic fabrication of 3-D structures by spontaneous folding of tapes," *J. Amer. Chem. Soc.*, vol. 128, no. 29, pp. 9314–9315, Jul. 2006.

[11] H. K. Ye, Z. Y. Gu, T. Yu, and D. H. Gracias, "Integrating nanowires with substrates using directed assembly and nanoscale soldering," *IEEE Trans. Nanotechnol.*, vol. 5, no. 1, pp. 62–66, Jan. 2006.

[12] M. Boncheva, S. A. Andreev, L. Mahadevan, A. Winkleman, D. R. Reichman, M. G. Prentiss, S. Whitesides, and G. M. Whitesides, "Magnetic self-assembly of three-dimensional surfaces from planar sheets," *Proc. Nat. Acad. Sci. U.S.A.*, vol. 102, no. 11, pp. 3924–3929, Mar. 2005.

[13] H. O. Jacobs, A. R. Tao, A. Schwartz, D. H. Gracias, and G. M. Whitesides, "Fabrication of a cylindrical display by patterned assembly," *Science*, vol. 296, no. 5566, pp. 323–325, Apr. 2002.

[14] D. H. Gracias, J. Tien, T. L. Breen, C. Hsu, and G. M. Whitesides, "Forming electrical networks in three dimensions by self-assembly," *Science*, vol. 289, no. 5489, pp. 1170–1172, Aug. 2000.

[15] Y. K. Hong and R. R. A. Syms, "Stability of surface tension self-assembled 3D MOEMS," *Sens. Actuators A, Phys.*, vol. 127, no. 2, pp. 381–391, Mar. 2006.

[16] R. R. A. Syms, E. M. Yeatman, V. M. Bright, and G. M. Whitesides, "Surface tension-powered self-assembly of microstructures—The state-of-the-art," *J. Microelectromech. Syst.*, vol. 12, no. 4, pp. 387–417, Aug. 2003.

[17] T. H. Galow, A. K. Boal, and V. M. Rotello, "A 'building block' approach to mixed-colloid systems through electrostatic self-organization," *Adv. Mater.*, vol. 12, no. 8, pp. 576–579, 2000.

[18] J. Kolny, A. Kornowski, and H. Weller, "Self-organization of cadmium sulfide and gold nanoparticles by electrostatic interaction," *Nano Lett.*, vol. 2, no. 4, pp. 361–364, 2002.

[19] X. Q. Wang, K. Naka, M. F. Zhu, H. Itoh, and Y. Chujo, "Microporous nanocomposites of Pd and Au nanoparticles via hierarchical self-assembly," *Langmuir*, vol. 21, no. 26, pp. 12 395–12 398, Dec. 2005.

[20] B. A. Grzybowski, A. Winkleman, J. A. Wiles, Y. Brumer, and G. M. Whitesides, "Electrostatic self-assembly of macroscopic crystals using contact electrification," *Nature Mater.*, vol. 2, no. 4, pp. 241–245, Apr. 2003.

[21] A. M. Kalsin, M. Fialkowski, M. Paszewski, S. K. Smoukov, K. J. M. Bishop, and B. A. Grzybowski, "Electrostatic self-assembly of binary nanoparticle crystals with a diamond-like lattice," *Science*, vol. 312, no. 5772, pp. 420–424, Apr. 2006.

[22] A. M. Kalsin, A. O. Pinchuk, S. K. Smoukov, M. Paszewski, G. C. Schatz, and B. A. Grzybowski, "Electrostatic aggregation and formation of core-shell suprastructures in binary mixtures of charged metal nanoparticles," *Nano Lett.*, vol. 6, no. 9, pp. 1896–1903, Sep. 2006.

[23] S. O. Lumsdon, E. W. Kaler, and O. D. Velev, "Two-dimensional crystallization of microspheres by a coplanar AC electric field," *Langmuir*, vol. 20, no. 6, pp. 2108–2116, Mar. 2004.

[24] A. Yethiraj, J. H. J. Thijssen, A. Wouterse, and A. van Blaaderen, "Large-area electric-field-induced colloidal single crystals for photonic applications," *Adv. Mater.*, vol. 16, no. 7, pp. 596–600, 2004.

[25] W. D. Ristenpart, I. A. Aksay, and D. A. Saville, "Electrically guided assembly of planar superlattices in binary colloidal suspensions," *Phys. Rev. Lett.*, vol. 90, no. 12, p. 128 303, Mar. 2003.

[26] L. M. Demers and C. A. Mirkin, "Combinatorial templates generated by dip-pen nanolithography for the formation of two-dimensional particle arrays," *Angew. Chem., Int. Ed. Engl.*, vol. 40, no. 16, pp. 3069–3071, Aug. 2001.

[27] N. Naujoks and A. Stemmer, "Micro- and nanoxerography in liquids—Controlling pattern definition," *Microelectron. Eng.*, vol. 78/79, pp. 331–337, Mar. 2005.

[28] H. P. Zheng, M. C. Berg, M. F. Rubner, and P. T. Hammond, "Controlling cell attachment selectively onto biological polymer-colloid templates using polymer-on-polymer stamping," *Langmuir*, vol. 20, no. 17, pp. 7215–7222, Aug. 2004.

[29] C. R. Barry, N. Z. Lwin, W. Zheng, and H. O. Jacobs, "Printing nanoparticle building blocks from the gas phase using nanoxerography," *Appl. Phys. Lett.*, vol. 83, no. 26, pp. 5527–5529, Dec. 2003.

[30] C. R. Barry, J. Gu, and H. O. Jacobs, "Charging process and Coulomb-force-directed printing of nanoparticles with sub-100-nm lateral resolution," *Nano Lett.*, vol. 5, no. 10, pp. 2078–2084, Oct. 2005.

[31] Y. N. Xia and G. M. Whitesides, "Soft lithography," *Annu. Rev. Mater. Sci.*, vol. 28, pp. 153–184, 1998.

[32] J. M. Meek and J. D. Craggs, *Electrical Breakdown of Gases*. Oxford, U.K.: Clarendon, 1953.

[33] K. L. Johnson, K. Kendall, and A. D. Roberts, "Surface energy and the contact of elastic solids," *Proc. R. Soc. Lond. A, Math. Phys. Sci.*, vol. 324, no. 1558, pp. 301–313, Sep. 1971.

[34] K. Kendall, *Molecular Adhesion and its Applications: The Sticky Universe*. New York: Plenum, 2001.

[35] D. S. Rimai, D. J. Quesnel, and A. A. Busnaina, "The adhesion of dry particles in the nanometer to micrometer-size range," *Colloids Surf., A Physicochem. Eng. Asp.*, vol. 165, no. 1–3, pp. 3–10, May 2000.

[36] P. N. Pusey, W. Vanmegen, P. Bartlett, B. J. Ackerson, J. G. Rarity, and S. M. Underwood, "Structure of crystals of hard colloidal spheres," *Phys. Rev. Lett.*, vol. 63, no. 25, pp. 2753–2756, Dec. 1989.
[37] L. I. Berger, Ed., *CRC Handbook of Chemistry and Physics*. Boca Raton, FL: CRC Press, 2000.
[38] U. Lachish and I. T. Steinberger, "Electrical current measurements on polystyrene films," *J. Phys. D, Appl. Phys.*, vol. 7, no. 1, pp. 58–68, Jan. 1974.
[39] N. Bowden, S. Brittain, A. G. Evans, J. W. Hutchinson, and G. M. Whitesides, "Spontaneous formation of ordered structures in thin films of metals supported on an elastomeric polymer," *Nature*, vol. 393, no. 6681, pp. 146–149, May 1998.
[40] Y. N. Xia, X. M. Zhao, E. Kim, and G. M. Whitesides, "A selective etching solution for use with patterned self-assembled monolayers of alkanethiolates on gold," *Chem. Mater.*, vol. 7, no. 12, pp. 2332–2337, Dec. 1995.
[41] Y. N. Xia, E. Kim, M. Mrksich, and G. M. Whitesides, "Microcontact printing of alkanethiols on copper and its application in microfabrication," *Chem. Mater.*, vol. 8, no. 3, pp. 601–603, Mar. 1996.

Adam Winkleman received the B.S. degree in chemistry from the University of Southern California, Los Angeles, where he worked in the laboratory of Prof. L. Dalton, and the Ph.D. degree in chemistry under the direction of Prof. G. M. Whitesides. His thesis work explores the manipulation and assembly of microscopic particles and cells using electrostatic and magnetic forces.

He was a Postdoctoral Fellow in the Department of Chemical Physics, Weizmann Institute of Science, Rehovot, Israel. He is currently a Senior Scientist with Nanoterra Inc., Cambridge, MA.

Logan S. McCarty received the A.B. degree in chemistry from Harvard University, Cambridge, MA, where he worked in the laboratory of Prof. R. H. Holm, and the Ph.D. degree in chemistry under the direction of Prof. G. M. Whitesides. His thesis work explores the synthesis and characterization of ionic electrets: dielectric materials that bear a net electrostatic charge due to an imbalance between the number of cationic charges and anionic charges in the material.

He is currently an Assistant Dean at the Harvard College, Harvard University.

Ting Zhu received the Ph.D. degree in mechanical engineering from the Massachusetts Institute of Technology, Boston, in 2004.

He spent a year as a Postdoctoral Associate at Harvard University, Cambridge, MA, where he studied the electrostatics of guided self-assembly. He is currently an Assistant Professor with the George W. Woodruff School of Mechanical Engineering, Georgia Institute of Technology, Atlanta. His research is focused on the modeling and simulation of mechanical behavior of materials at the nanoscale to macroscale.

He is a member of the American Society of Mechanical Engineers.

Douglas B. Weibel received the B.S. degree in chemistry from the University of Utah, Salt Lake City (with Prof. C. Dale Poulter), in 1996 and the Ph.D. degree in chemistry from Cornell University, Ithaca, NY (with Prof. J. Meinwald), in 2002.

During 1996–1997, he was a Fulbright Fellow at Tohoku University, Sendai, Japan (with Prof. Y. Yamamoto). From 2002 to 2006, he was a Postdoctoral Fellow with George M. Whitesides at Harvard University, Cambridge, MA. He is currently an Assistant Professor of biochemistry at the University of Wisconsin, Madison. His research interests include biochemistry, biophysics, chemical biology, materials science and engineering, and microbiology.

Zhigang Suo received the bachelor's degree in engineering mechanics from Xi'an Jiaotong University, Xi'an, China, in 1985 and the Ph.D. degree in engineering science from Harvard University, Cambridge, MA, in 1989.

He is an Allen E. and Marilyn M. Puckett Professor of mechanics and materials in the School of Engineering and Applied Sciences, Harvard University. In 1989, he joined the faculty of the University of California, Santa Barbara, and established a group studying the mechanics of small structures. The group moved to Princeton University, Princeton, NJ, in 1997 and to Harvard University in 2003. His work centers on the mechanical behavior of small structures, whose basic processes include deformation of materials, fracture of structures, and transport of matter and whose applications are mainly concerned with thin-film structures in microelectronics and large-area electronics. He has coauthored over 190 archival papers.

Dr. Suo received the Pi Tau Sigma Gold Medal and the Special Achievement Award for Young Investigators in Applied Mechanics from the American Society of Mechanical Engineers (ASME). He is a Fellow of ASME.

George M. Whitesides received the A.B. degree from Harvard University, Cambridge, MA, in 1960, and the Ph.D. degree from the California Institute of Technology, Pasadena, in 1964.

He was a Mallinckrodt Professor of Chemistry from 1982 to 2004. He is currently a Woodford L. and Ann A. Flowers University Professor. Prior to joining the faculty of Harvard University in 1992, he was a member of the chemistry faculty of the Massachusetts Institute of Technology, Cambridge. His research interests include physical and organic chemistry, materials science, biophysics, complexity, surface science, microfluidics, self-assembly, microtechnology and nanotechnology, and cell-surface biochemistry.